TU Delft

Delft University of Technology

Document Version
Final published version

Licence
Dutch Copyright Act (Article 25fa)

Citation (APA)
Flessati, L., Habib, F., Wu, K. W., Liu, H., & Pisanò, F. (2026). Conceptualising the lateral response of monopiles in sand to monotonic and cyclic loading: A SANISAND-MS 3D FE investigation. *Computers and Geotechnics*, *195*, Article 108069. https://doi.org/10.1016/j.compgeo.2026.108069

Important note
To cite this publication, please use the final published version (if applicable).
Please check the document version above.

Copyright
In case the licence states “Dutch Copyright Act (Article 25fa)”, this publication was made available Green Open Access via the TU Delft Institutional Repository pursuant to Dutch Copyright Act (Article 25fa, the Taverne amendment). This provision does not affect copyright ownership.
Unless copyright is transferred by contract or statute, it remains with the copyright holder.

Sharing and reuse
Other than for strictly personal use, it is not permitted to download, forward or distribute the text or part of it, without the consent of the author(s) and/or copyright holder(s), unless the work is under an open content license such as Creative Commons.

Takedown policy
Please contact us and provide details if you believe this document breaches copyrights.
We will remove access to the work immediately and investigate your claim.

This work is downloaded from Delft University of Technology.

Computers and Geotechnics 195 (2026) 108069

Contents lists available at ScienceDirect

Computers and Geotechnics

journal homepage: www.elsevier.com/locate/compgeo

Research paper

Conceptualising the lateral response of monopiles in sand to monotonic and cyclic loading: A SANISAND-MS 3D FE investigation

Luca Flessati [a], Firman Habib [b], Kuen-Wei Wu [b], Haoyuan Liu [c,*,1], Federico Pisanò [d,2]

[a] Delft University of Technology, Delft, The Netherlands
[b] Van Oord, Rotterdam, The Netherlands
[c] Beihang University, Beijing, China
[d] Norwegian Geotechnical Institute, Boston, USA

ARTICLE INFO

Keywords:
Offshore wind
Monopiles
Finite element modelling
Cyclic loading
Sand

ABSTRACT

The design of monopile foundations for offshore wind turbines is often governed by lateral tilt under monotonic and cyclic loading, commonly assessed using distributed (spring-based) soil-reaction models. While these models are well established for monotonic loading, their extension to cyclic conditions – and their acceptance in industry – remains limited. As part of a broader research programme on cyclic soil-reaction modelling, this paper supports such developments through non-linear 3D FE analyses of monopile response in sand under monotonic and cyclic loading. The SANISAND-MS constitutive model is employed to capture the drained cyclic behaviour of the sand, including ratcheting. Extensive parametric studies are performed to investigate the combined effects of geometric, geotechnical, and loading conditions. The results confirm well-known aspects of monopile mechanics while also highlighting less-studied features, including the relative contributions of different (cyclic) soil-reaction components (within the PISA framework) and the quantitative influence of relative monopile-soil stiffness on both monotonic and cyclic response. Finally, the study proposes interpolation laws synthesising the numerical findings, which can aid in conceptualising monopile lateral behaviour, guiding future experimental campaigns, and, very importantly, informing the development and validation of simplified soil-reaction models.

1. Introduction

Wind energy production continues to grow to meet the global demand for renewable power, and offshore wind turbines (OWTs) provide an efficient means of harnessing this resource. Large steel piles – commonly referred to as "monopiles" – are currently the most prevalent foundation type for OWTs due to their cost-effectiveness and suitability for mass production. Among the various design considerations, evaluating monopile tilt under lateral loading remains a key aspect of serviceability assessment.

With a particular focus on cyclic loading conditions, several numerical approaches are available to predict lateral tilt. These include – listed in order of increasing dimensionality – lumped macroelements (also known as 0D models) (Li et al., 2016; Page et al., 2018, 2019), distributed soil-reaction spring models used with 1D pile analyses (Fuentes et al., 2021; Beuckelaers et al., 2020; Kementzetzidis et al., 2022; Zha et al., 2022), and fully 3D continuum models (Achmus et al., 2009; Staubach and Wichtmann, 2020; Liu et al., 2022; Jostad et al., 2023; Li et al., 2023, 2025).

3D finite element (FE) simulations offer the greatest versatility for analysing the influence of governing factors, including pile geometry, load history, soil behaviour, and soil stratigraphy/heterogeneity. However, they typically involve high computational costs, making long-term monopile simulations (extending up to 10^7–10^8 cycles, Houlsby (2016)) impractical for multiple foundation sites (Pisanò, 2019). Therefore, the abovementioned simplified approaches (0D or 1D models) are generally preferred for handling large cycle numbers (Abadie et al., 2023).

Although computationally attractive, these modelling approaches require the adoption of appropriate upscaled constitutive relationships to capture soil–structure interaction mechanisms. The development of such laws necessitates their formulation, calibration, and validation against observed pile response under both monotonic and cyclic loading. A major obstacle in this effort is the scarcity of full-scale tests,

* Corresponding author.
E-mail addresses: L.Flessati@tudelft.nl (L. Flessati), Firman.Habib@vanoord.com (F. Habib), Wayne.Wu@vanoord.com (K.-W. Wu), liuhaoyuan24@buaa.edu.cn (H. Liu), federico.pisano@ngi.no (F. Pisanò).
[1] Formerly Norwegian Geotechnical Institute, Oslo, Norway.
[2] Formerly Delft University of Technology, Delft, The Netherlands.

https://doi.org/10.1016/j.compgeo.2026.108069
Received 26 September 2025; Received in revised form 10 February 2026; Accepted 9 March 2026
Available online 23 March 2026
0266-352X/© 2026 Elsevier Ltd. All rights are reserved, including those for text and data mining, AI training, and similar technologies.

coupled with the difficulties of exploiting available experimental data to inform specific modelling choices and calibration steps. In regimes where soil behaviour remains linear, analytical calibration expressions can be established – see, for example, Higgins et al. (2013) and He and Kaynia (2024) for 0D and 1D pile analyses, respectively. However, the intrinsic non-linearity of soil behaviour, particularly under sufficiently large external loads, prevents the development of simple calibration procedures, making the use of experimental evidence essential for producing reliable models and attaining wide industry acceptance.

The execution of small-scale model tests – either under 1 g conditions or in a geotechnical centrifuge – as well as medium- or full-scale field tests, is now entirely feasible and widely employed, as evidenced by the substantial body of literature available (LeBlanc et al., 2010; Klinkvort and Hededal, 2013; Li et al., 2015; Abadie et al., 2019; Richards et al., 2020; McAdam et al., 2020; Byrne et al., 2020a,b; Li et al., 2022; Wang et al., 2022a; Kementzetzidis et al., 2023a; Liu et al., 2024). However, time and budget constraints typically impose on these experimental programs limitations on the number of tests, so that only selected combinations of pile geometries and soil properties can be considered. Furthermore, the small scale of tested model piles means that even miniaturised sensors used to measure local responses and soil–structure interaction forces may influence the results, making a detailed evaluation of the local processes near the pile challenging. As a consequence, it is difficult to perform truly exhaustive and internally consistent investigations – both in terms of experimental methods and test setups – to unravel all quantitative dependencies of monopile response features on the full range of governing factors.

For instance, although monopiles are often described as responding to lateral loading primarily through rigid rotation, real designs often fall, depending on site-specific soil conditions, into an intermediate regime in which the lateral response involves a combination of rigid rotation and flexural deformation (Abadie et al., 2019). This makes it challenging to conceptualise and systematise the various levels of such transitional behaviour, particularly under complex cyclic loading conditions. In this regard, the problem of quantitatively determining the influence of relative pile–soil stiffness on cyclic response characteristics has not yet been conclusively addressed (Wang et al., 2022b).

The industry's need for design approaches that are sufficiently simple yet reliable and robust has, in recent years, led to the development of the PISA 1D analysis framework for monopiles, originally proposed to reproduce the monotonic lateral response of monopiles in sand (Byrne et al., 2019). The fundamental idea behind this framework is to extend standard subgrade-reaction modelling – initially developed for slender, flexible piles – to the case of stiff OWT monopiles. This is accomplished by introducing additional soil-reaction components, including the distributed moment along the pile shaft and the base force and moment, alongside the conventional lateral soil reaction. If appropriately calibrated, the PISA model can successfully reproduce the monotonic system response, both in terms of load–displacement behaviour and bending-moment distributions. However, in its current form it is not equipped to capture key aspects of cyclic behaviour, such as the progressive accumulation of irreversible displacements.

In light of the above gaps, this paper presents research conducted as part of the MIDAS project, a research initiative aimed at advancing physical and numerical modelling capabilities to improve monopile design approaches (Pisanò et al., 2022, 2025). MIDAS' overarching objective is to develop a cyclic soil-reaction model for 1D monopile analysis, informed by centrifuge load tests and 3D FE simulations, and to propose robust calibration procedures to facilitate its broad application in industrial offshore wind projects. This contribution leverages an advanced 3D FE modelling framework incorporating the memory-enhanced SANISAND-MS constitutive model (Liu et al., 2019) to: (i) characterise the mechanical processes occurring near the pile under monotonic and cyclic loading; (ii) quantify the influence of the different soil-reaction components defined within the PISA 1D monopile analysis framework; (iii) assess the impact of pile geometry and soil mechanical properties on the cyclic accumulation of displacements and rotations; and (iv) provide a set of numerical results for benchmarking simplified soil–monopile interaction models.

A validated and computationally robust 3D analysis tool enables consistent parametric exploration of the many factors that govern monopile lateral response and supports the identification of fundamental relationships between key response features – such as the rate of cyclic tilt accumulation – and governing parameters, such as the relative pile–soil stiffness, over a realistic range of conditions. The ultimate contribution of this paper is therefore both methodological and practical, in that it provides benchmark results and interpolation relationships derived from numerical procedures that are now readily accessible to practitioners beyond the academic research community.

2. 3D FE modelling of laterally loaded monopiles in sand

2.1. 3D FE model setup

To analyse the lateral response of piles in sand, a series of 3D non-linear finite element (FE) simulations were performed using Plaxis 3D, following the approach of Pisanò et al. (2024). A steel tubular pile of diameter D was embedded in a homogeneous dry sand layer. The total pile length consisted of both the embedded length (L) and the above-ground length (h). The soil domain used in the numerical analyses (Fig. 1) was defined based on the monopile geometry: the horizontal dimensions were set relative to the pile diameter ($30D$ and $15D$), while the vertical extent was set to four times the embedded length ($4L$). The symmetry inherent in the lateral loading of a cylindrical structure was exploited to model only half of the system, thereby reducing computational costs.

The soil domain was discretised into approximately 16,000 10-node tetrahedral elements, with finer elements near the pile (approximately $0.125D$) to capture larger strain gradients. The pile was modelled using approximately 1000 6-node triangular plate elements, with interface elements incorporated to simulate soil–pile interaction. In the normal direction, the interface elements exhibited a perfectly brittle response under tension and an elastic response under compression. To ensure that the interface stiffness value do not significantly affect the numerical results, it was set equal to five times that of the surrounding soil in a way to ensure a "nearly rigid" behaviour. In the tangential direction, the interface elements followed a "rigid"-perfectly plastic behaviour. The yield locus was defined by the Mohr–Coulomb criterion, with the friction angle taken as two-thirds of the soil critical state friction angle.

The domain size and element distribution were chosen to ensure accurate numerical solutions, leveraging experience from previous related research (Corciulo et al., 2017; Liu et al., 2022) and considering the higher accuracy of second-order tetrahedral elements used in Plaxis 3D (Pisanò et al., 2024). Boundary conditions were applied as follows: all displacements were constrained to zero at the base of the soil domain, while normal displacements were restricted along the vertical boundaries. A horizontal force H was applied at the pile head.

The quasi-static numerical analyses were conducted in the following stages:

1. **Stress initialisation** – The initial stress state was imposed using a k_0 procedure, where k_0 represents the at-rest lateral earth pressure coefficient.
2. **Pile installation** – The pile was assumed to be "wished-in-place", a common assumption when investigating pile installation effects is not the primary focus of the analysis (Hu et al., 2022; Liu et al., 2022).
3. **Lateral loading** – The horizontal force H was applied either monotonically or cyclically.

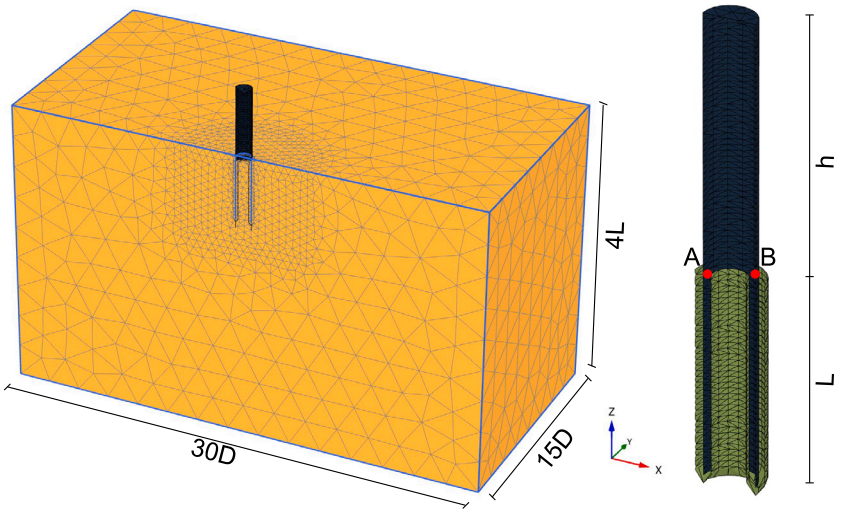


Fig. 1. Model geometry and FE discretisation.

Although the initial stress state – as resulting from soil unit weight and the pile installation process – quantitatively influences the lateral response of monopiles, prior studies have shown that these factors do not modify the general qualitative behaviour (Achmus et al., 2020; Liu et al., 2022; Pisanò et al., 2024). Consequently, the governing mechanisms, behavioural patterns, and the relative contributions of the soil reaction components – the main focus of this paper – are not expected to be significantly affected. Moreover, recent literature indicates that assuming a wished-in-place installation generally leads to conservative predictions of monopile lateral deflection under monotonic loading; under cyclic loading, installation effects are mostly confined to the early cycles and tend to vanish as cycling progresses (Staubach et al., 2020; Kementzetzidis et al., 2023b; Pisanò et al., 2024).

All cyclic numerical analyses were performed for 100 cycles; therefore, it would be imprudent to directly extrapolate these results to long-term monopile performance. Nevertheless, this limitation does not detract from the value of the findings presented in the following sections. The results serve to (i) elucidate fundamental geotechnical mechanisms and behavioural patterns and (ii) support mechanics-based enhancements of engineering design approaches (Pisanò, 2019) – insights that cannot be obtained from experimental datasets that are often inevitably restricted to specific geometries and soil conditions.

2.2. Material modelling and constitutive parameters

Steel monopiles were considered in this numerical study, each assigned standard material properties: Young's modulus of 200 GPa, Poisson's ratio of 0.3, and a unit weight of 78.5 kN/m^3. The pile wall thickness (t_p) was set to 10 cm.

The dry unit weight of the soil (γ_{dry}) was determined based on the target relative density of the sand (D_r) for each specific 3D model. This was computed assuming a specific gravity (G_s) of 2.67 and minimum and maximum void ratios of 0.64 and 1.07, respectively. These values were obtained from standard laboratory tests conducted on Geba sand, the reference sand type used throughout the MIDAS experimental programme (Wang et al., 2025). Geba sand is a silica-based, slightly silty, fine, poorly graded sand (D_{10}, D_{50}, and D_{60} equal 0.081 mm, 0.119 mm, and 0.129 mm, respectively), already used in previous physical modelling studies (Zhang and Askarinejad, 2019; Li et al., 2022).

The mechanical behaviour of Geba sand was modelled using the well-established SANISAND-MS model, originally developed by Liu et al. (2019). This model is an extension of the original SANISAND model by Dafalias and Manzari (2004). It preserves the advantages of bounding surface plasticity in simulating cyclic sand behaviour while enhancing accuracy in modelling cyclic strain accumulation through the introduction of a memory surface (Corti et al., 2016). SANISAND-MS has been successfully applied to cyclic soil–pile interaction problems and is gaining broad traction in cyclic 3D FE studies across the research community (Roy et al., 2024; Wen et al., 2025; Stastny et al., 2025; Liu et al., 2026a). The implementation used in this study follows the latest work outlined by Li et al. (2026), which was recently validated against cyclic pile load test data from Byrne et al. (2020a) by Pisanò et al. (2024).

Predictions obtained with the SANISAND-MS model depend on the adopted set of elastic and plastic parameters (Liu et al., 2019). The model employs a non-linear hypo-elastic formulation in which the shear modulus varies with both mean effective stress (p') and void ratio (e) through a dimensionless stiffness factor G_0, while the Poisson's ratio ν is kept constant. In the q–p' stress plane, the opening of the conical yield surface is controlled by the parameter m_Y, and its rotation about the apex is governed by the kinematic hardening rule. The critical-state stress ratio under general loading paths is defined based on its values in triaxial compression (M_c) and triaxial extension ($c \cdot M_c$, where c is the triaxial-extension multiplier). The critical state line in the e–p' plane is described by three parameters (λ_c, e_0, ξ), while the evolution of plastic stiffness during loading is controlled by the parameters h_0 and c_h. The distance between peak strength and the critical state is governed by the evolving state parameter ψ, as defined by Been and Jefferies (1985), together with the additional model parameter n_b. In the latest version of the model (Li et al., 2026), an additional parameter $M_c^{b,\max}$ is introduced to impose an upper bound on the mobilised peak strength associated with the bounding surface under triaxial compression, thereby preventing unrealistically high strength mobilisation in very dense states or under non-triaxial loading paths – in this regard, see also Taborda et al. (2020). Dilatancy is governed by two parameters, A_0 and n_d, where the former primarily regulates its magnitude and the latter controls its dependence on ψ. Under cyclic loading, dilatancy is additionally influenced by the cyclic parameter β and is indirectly affected by the memory-hardening mechanism, which governs cyclic strain accumulation through the parameters μ_0 and ζ.

The constitutive parameters for Geba sand were calibrated using experimental data from element soil tests and centrifuge pile load experiments. These tests were conducted at Deltares' laboratory (Delft, the Netherlands) as part of the MIDAS research programme (Wang et al., 2025; Peccin da Silva et al., 2026). The final calibrated parameters, tailored for the specific MIDAS centrifuge tests, are summarised in Table 1, with most values broadly falling within the same range as

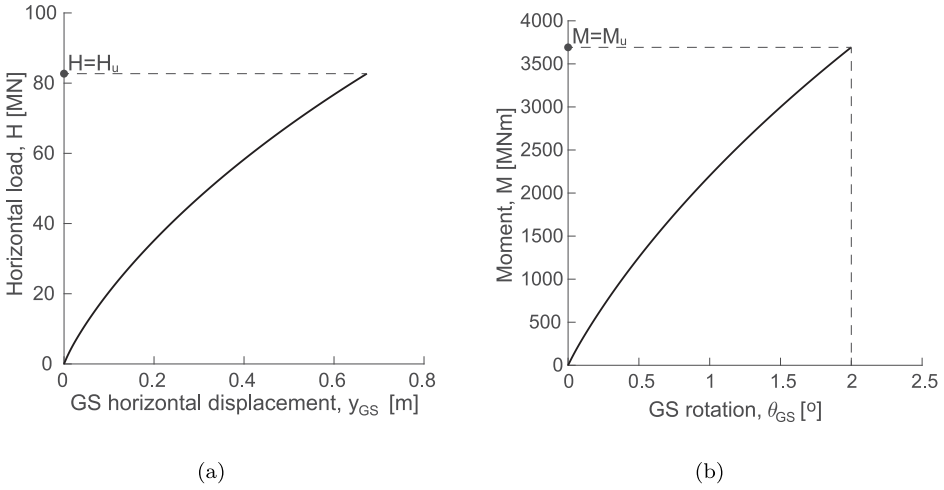


Fig. 2. Simulated monotonic monopile response: (a) load–displacement and (b) moment–rotation curves.

Table 1
Calibrated SANISAND-MS model parameters for Geba sand, based on Liu et al. (2026).

Elasticity		Strength and critical state							Yielding
G_0	ν	M_c	c	$M^b_{c,\max}$	n^b	λ_c	e_0	ξ	m_Y
400	0.05	1.25	0.70	1.9	0.96	0.0015	0.935	0.7	0.1

Plastic modulus		Dilatancy		Cyclic/memory effects		
h_0	c_h	A_0	n^d	μ_0	ζ	β
8.64	1.09	1.1	0.75	500	0.0001	1

those identified for Karlsruhe sand (Liu et al., 2019; Li et al., 2026), Ottawa 20/30 sand (Liu and Pisanò, 2019), and Dunkirk sand (Pisanò et al., 2024).

While the calibration and validation work is extensively reported in Liu et al. (2026), the key aspects relevant to the present study are summarised in Appendix, demonstrating that the 3D FE results presented herein build on a sound numerical model – previously validated against experimental observations of monopile behaviour under monotonic and cyclic loading in uniform sand.

3. Numerical results of monopile behaviour – a reference case

To investigate the mechanical response of monopiles under monotonic and cyclic loads, numerical parametric studies were performed. This section presents and interprets the results of a selected reference case (D = 9 m, L/D = 4, h/D = 5, D_r = 90%) to highlight general, recurring system response features.

3.1. Response to lateral monotonic loading

Fig. 2 presents the numerical simulation results of the monopile subjected to a monotonically increasing lateral load, shown through the H–y_{GS} (Fig. 2a) and M–θ_{GS} (Fig. 2b) relationships. The surface moment is computed as $M = H \cdot h$, whereas y_{GS} and θ_{GS} denote the horizontal displacement and rotation at the ground surface, respectively. The rotation θ_{GS} is obtained by dividing the differential vertical displacement between points A and B in Fig. 1 by the pile diameter.

Both curves exhibit a continuous increase, indicating no clear mechanical failure. In this study, the ultimate condition is conventionally

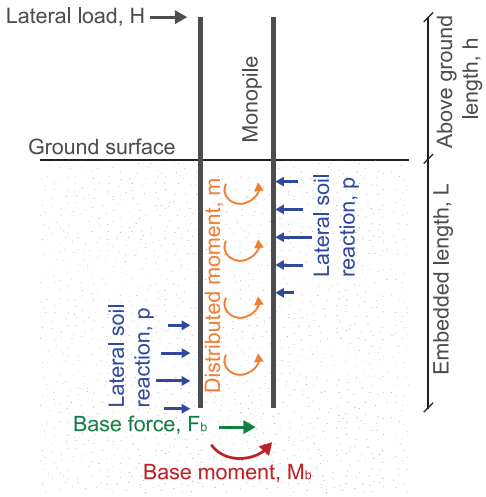


Fig. 3. Idealised soil reaction components for short monopiles. Forces and displacements positive rightward; moments and rotations positive clockwise.

defined as $\theta_{GS} = 2°$ (Richards et al., 2020), corresponding to ultimate values of $H = H_u = 82.7$ MN and $M = M_u = 3721$ MNm (Fig. 2).

Modern OWT monopiles are relatively short with a large diameter. As noted by Burd et al. (2020), their response is influenced by not only the lateral soil reaction p, but also the distributed moment m (arising from shear stresses due to relative vertical soil–pile movement), and by the base force and moment (F_B and M_B). These four components (illustrated in Fig. 3) were derived from 3D FE simulations. The reactions p and m were calculated from nodal force resultants along the pile perimeter, while F_B and M_B were deduced by enforcing equilibrium in translation and rotation, once the other contributions were known.

Fig. 4 displays the lateral p–y and rotational m–θ responses at varying depths z. Here, y denotes local horizontal displacement and θ the corresponding rotation.

At depths beyond 13 m (z/D> 0.36), the p–y curves increase monotonically, indicating the absence of local failure. Shallower depths exhibit different behaviour: at 6 m, the response plateaus (ductile response), while at 4–5 m, softening is observed (brittle response), suggesting local yielding and stress redistribution. Although these effects do not compromise overall pile stability due to the system's redundancy, they highlight limitations in simplified analytical p–y models (API, 2010; Li et al., 2014; DNV, 2016; Burd et al., 2020; Wang et al., 2022a), which often neglect such non-linear interactions. While

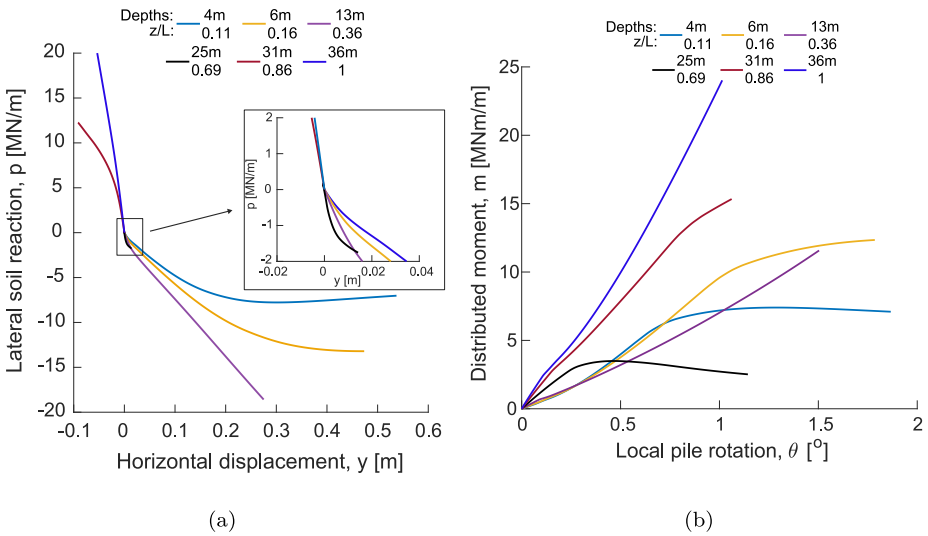


Fig. 4. Distributed soil reactions under monotonic loading: (a) lateral reaction (p–y) and (b) moment reaction (m–θ) at various depths.

overall load–displacement predictions remain accurate (Burd et al., 2020), local bending behaviour may be misrepresented.

The m–θ curves confirm that the pile is not entirely rigid. Rotations decrease with depth, reducing from 2° at the surface to approximately 1° at 36 m. Softening at 5–6 m mirrors the p–y behaviour, and further reductions at 25 m suggest a downward shift in the centre of rotation.

To clarify these trends, Fig. 5 presents the local soil response immediately next to the pile at selected depths using q–p' (normalised for representation purpose with respect to the geostatic effective mean stress p'_0) and e–p' plots, where p' denotes the effective mean stress, $q = \sqrt{(3/2)\, s_{ij} s_{ij}}$ is the deviatoric stress magnitude, and e is the void ratio. At 4 m depth, the compressed side (red in Fig. 5a and d) exhibits an almost linear stress path that reaches a peak before decreasing, accompanied by dilation. The decompressed side (blue) instead shows a pronounced reduction in stress and significant volume expansion. At 6 m, the compressed-side response (red in Fig. 5b and e) remains similar to that at 4 m, but the decompressed side behaves differently: after an initial drop, p' begins to increase. This contrast in decompressed-side behaviour explains the differences observed in the p–y trends at 4 m and 6 m. At 36 m depth, the response on both sides of the pile involves only minor void-ratio changes, and the sand remains far from the critical state, which allows the corresponding p–y curve to increase monotonically. Further discussion of soil stress paths around monopiles under monotonic lateral loading can be found in Cheng et al. (2023).

Fig. 6 illustrates the pile base response in terms of F_B–y_B and M_B–θ_B relationships, where y_B and θ_B represent base horizontal displacement and rotation. The sign convention follows Fig. 3, with positive values aligned with the applied load H and moment M. Both curves are nearly linear, suggesting that the ultimate condition ($\theta_{GS} = 2°$) occurs while irreversible deformations at the pile base remain rather limited.

To further evaluate the contribution of soil reactions to global pile behaviour, Fig. 7 shows bar charts of normalised force and moment components. Fig. 7a illustrates the evolution of F_B and P (the resultant lateral soil reaction) with respect to H/H_u, while Fig. 7b shows the evolution of M_B, M_{FB} (moment due to F_B), M_P (moment from lateral reactions), and M_D (moment from distributed m) as a function of M/M_u. The contribution of F_B increases significantly with the external load amplitude, reaching approximately 35% of H_u at (conventional) ultimate conditions. Its associated moment M_{FB} reaches 28% of M_u. The distributed moment M_D also increases, though it remains comparatively smaller (10% of M_u at ultimate). Conversely, M_B contributes minimally, remaining below 1%.

These findings highlight the necessity of including both F_B and M_D in simplified models to capture global pile response accurately. However, the negligible role of M_B in this case suggests it may be omitted without compromising accuracy. This conclusion, though, is specific to the present configuration and may not generalise across all pile geometries and soil conditions. This will be discussed in the following.

3.2. Response to lateral cyclic loading

During their operational lifetime, OWT monopiles are subjected to irregular loads with varying amplitudes, asymmetries, directions, and frequencies. Although few studies to date have captured all (or part of) these complexities (Richards et al., 2020; Abadie et al., 2023; Li et al., 2023; Abu-Kassab et al., 2025), current practice and much of the literature typically simplify environmental loading as regular, single-amplitude cyclic loads (LeBlanc et al., 2010; Klinkvort and Hededal, 2013; Abadie et al., 2019; Li et al., 2022). Within this framework, each cyclic load is characterised by its mean value and amplitude, or alternatively, by the non-dimensional load factors for amplitude (ζ_b) and asymmetry (ζ_c), as introduced in LeBlanc et al. (2010):

$$\zeta_b = \frac{M_{\max}}{M_u} \qquad \zeta_c = \frac{M_{\min}}{M_{\max}} \tag{1}$$

where $M_{\max}$ and $M_{\min}$ denote the maximum and minimum moments applied within each load cycle. The same formulation can be applied to lateral force loads with unaltered value of the two dimensionless factors.

The geotechnical serviceability of monopiles may often be governed by the lateral tilt accumulated during cyclic loading. Accurate prediction of rotation and displacement at the ground surface ($\Delta\theta_{GS}$ and Δy_{GS}, respectively) is therefore essential. These quantities are typically expressed relative to their first-cycle values, $\theta_{GS,0}$ and $y_{GS,0}$, as a function of the number of cycles N.

Fig. 8 illustrates the accumulation of ground surface rotation for 1 g small-scale Test 18, reported in LeBlanc et al. (2010) (pile diameter and lenght 80 mm and 360 mm, respectively, sand's relative density 38% and one-way cycles), plotted on a bi-logarithmic scale. The experimental results follow an approximately bilinear trend: a steeper initial branch ($N < 100$), followed by a flatter second branch ($N > 100$). LeBlanc et al. (2010) fitted the latter with a power law:

$$\frac{\Delta\theta_{GS}}{\theta_{GS,0}} = T_{GS,b} T_{GS,c} N^{T_{GS,\alpha}} \tag{2}$$

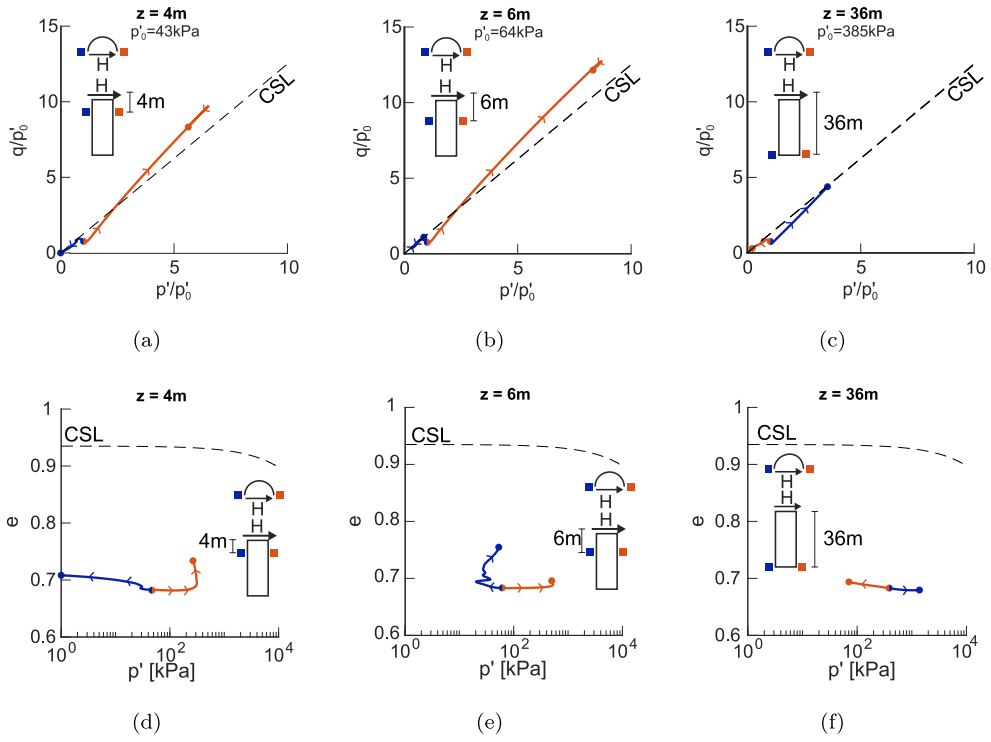


Fig. 5. Local soil response at depths of (a,d) 4 m, (b,e) 6 m, and (c,f) 36 m under monotonic loading. p'_0 is the geostatic effective pressure. The normalisation in the $q - p'$ planes is introduced to better visualise the results.

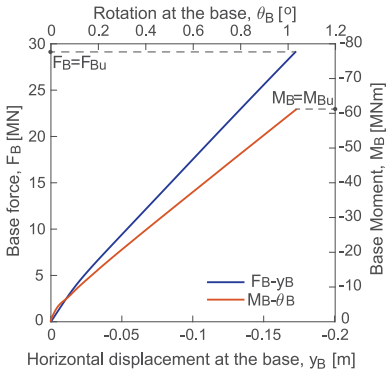


Fig. 6. Simulated pile base response: base shear force vs. base displacement and base moment vs. base rotation.

Here, $T_{GS,b}$ depends on ζ_b and relative density; $T_{GS,c}$ is a function of ζ_c, and equals 1 when $\zeta_c = 0$; $T_{GS,\alpha}$ was set to 0.31. The solid line in Fig. 8 corresponds to $T_{GS,b} = 0.19$, $T_{GS,c} = 1$, which closely matches the experimental trend beyond 100 cycles. The initial segment ($N < 100$) is also well-represented by a power law, albeit with different coefficients. The dashed line reflects $T_{GS,b} = 0.12$, $T_{GS,\alpha} = 0.45$, consistent with values used by Liu et al. (2022) for 100-cycle 3D FE simulations. It should also be noted that the framework proposed by LeBlanc et al. (2010) implicitly assumes an indefinite accumulation of pile rotation under single-amplitude cyclic loading, without accounting for the possible saturation of this trend (*shakedown response*). Experimental evidence, for instance from Peccin da Silva et al. (2026), shows that such shakedown behaviour can occur for monopiles in very dense sand (relative density approaching 100%). The same simplifying assumption is adopted here in order to extend the analysis of LeBlanc et al. (2010), but no systematic investigation of the ratcheting-to-shakedown transition is attempted, as this would require considerably longer cyclic load histories and substantially higher computational effort.

The following analysis presents FE results from two simulations based on the reference geometry and soil properties described in Section 3.1, both with $\zeta_c = 0$ but different ζ_b values: 0.1 and 0.4.

This framework was extended to examine the accumulation of displacement and rotation not only at the ground surface, but also along the pile shaft and at the pile base. This approach provides a comprehensive view of the mechanical response during cyclic loading and supports the development of simplified design models. A similar methodology was also applied to analyse the evolution of various soil reaction components, which is expected to assist in advancing cyclic design models, including those based on stiffness degradation (Reese et al., 1974; Little and Briaud, 1988; Long and Vanneste, 1994).

Fig. 9 summarises the ground surface response: load–displacement and moment–rotation curves, and the cyclic accumulation of lateral displacement and rotation. As anticipated, both lateral displacement and rotation accumulate progressively with increasing load cycles. When plotted on a bi-logarithmic scale, the accumulated quantities exhibit approximately linear behaviour, and the curves for different load cases are nearly parallel. The load–displacement and moment–rotation plots also reveal notable differences in unloading behaviour: for $\zeta_b = 0.1$, the unloading paths are nearly linear, whereas for $\zeta_b = 0.4$, a mild non-linearity becomes evident.

These trends highlight the importance of accounting for rotational hardening in both macroelement models and soil–pile interaction frameworks. Incorporating this behaviour is key to reliably simulating the cyclic response of soils in these modelling approaches (Houlsby et al., 2017; Page et al., 2019; Kementzetzidis et al., 2022).

Consistent with the formulation of LeBlanc et al. (2010), the accumulation of rotation was interpolated using Eq. (2). A similar power-law expression was adopted for displacement:

$$\Delta y_{GS} = Y_{GS,b} Y_{GS,c} N^{Y_{GS,\alpha}} \tag{3}$$

where $Y_{GS,b}$, $Y_{GS,c}$, and $Y_{GS,\alpha}$ mirror the roles of their rotational counterparts in Eq. (2).

The dashed lines in Fig. 9 represent results fitted using Eqs. (2) and (3), with coefficients listed in Table 2. In agreement with LeBlanc

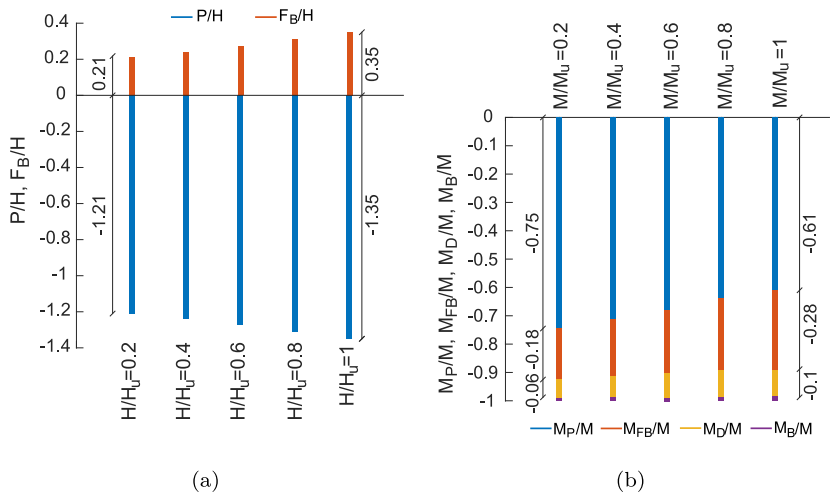


Fig. 7. Distribution of soil reaction components under monotonic loading: (a) force contributions (F_B, P) vs. H, and (b) moment contributions (M_P, M_{FB}, M_D, M_B) vs. M.

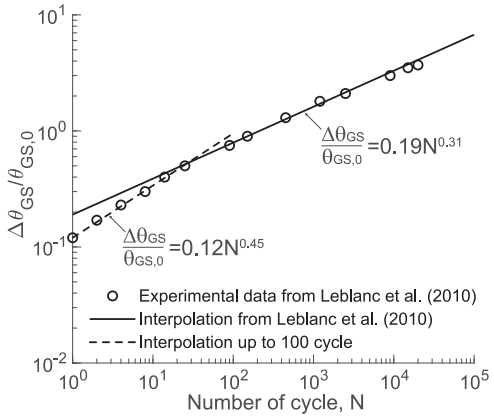


Fig. 8. Cyclic accumulation of monopile rotation at ground surface — Test 18 from LeBlanc et al. (2010): pile diameter 80 mm, length 360 mm, load eccentricity 430 mm, sand's relative density 38%, and 17,532 cycles with $\zeta_b = 0.52$ and $\zeta_c = 0$.

Table 2
Interpolation parameters used for the dashed lines in Fig. 9 ($Y_{GS,c} = T_{GS,c} = 1$ in all cases).

	$Y_{GS,b}$	$Y_{GS,\alpha}$	$T_{GS,b}$	$T_{GS,\alpha}$
$\zeta_b = 0.1$	0.01	0.55	0.006	0.55
$\zeta_b = 0.4$	0.04	0.55	0.026	0.55

et al. (2010), both $T_{GS,b}$ and $Y_{GS,b}$ increase with ζ_b, reflecting greater accumulation at higher load amplitudes. These coefficients are also expected to depend on soil relative density and pile geometry – only a single pile geometry was considered in LeBlanc et al. (2010)'s study. This dependency is further explored in the last section of the paper.

Since the numerical results yield nearly parallel curves in bi-logarithmic space, a common exponent of $T_{GS,\alpha} = Y_{GS,\alpha} = 0.55$ was adopted for all cases. This value aligns closely with that reported by Liu et al. (2022) for up to 100 cycles of FE analysis – in that previous study the SANISAND-MS parameters were calibrated for Karlsruhe sand.

The p–y curves shown in Fig. 10a are non-linear at all depths, and lateral displacement accumulates with each cycle. In the bi-logarithmic plot (Fig. 10b), accumulated displacement increases approximately linearly with N, with nearly parallel trends across depths—similar to those observed at the ground surface (Fig. 9c–d).

Interestingly, although the load amplitude remains constant across cycles, the maximum lateral reaction p_N does not (Fig. 10c). At some depths (e.g., 19 m, 36 m), p_N increases with cycling; at others (e.g., 5 m), it decreases. In certain locations (e.g., 13 m, 31 m), p_N initially rises then falls. This depth-dependent behaviour reflects stress redistribution along the pile due to complex soil–pile interactions. The results in Fig. 10 provide a useful benchmark for assessing simplified pile–soil models that aim to capture local interaction mechanisms (or for pointing out their limitations). These local mechanisms are governed by compatibility conditions and are not captured by standard simplified 1D models based on uncoupled non-linear springs. While the global response (e.g., load–displacement at ground level) may still be captured accurately with these simplified 1D models, inaccuracies in modelling the local lateral soil reactions may cause errors in predicting bending moment distributions.

Fig. 11 presents the numerical results for distributed moment responses under cyclic loading ($\zeta_b = 0.4$), including: m-θ curves, cyclic accumulation of rotation $\Delta\theta$ (normalised by θ_0), and the evolution of the distributed moment m_N normalised by m_0. These patterns closely mirror those previously observed in the p–y response (Fig. 10), highlighting similar complexities in capturing cyclic behaviour through simplified soil–pile interaction models.

Fig. 12 shows the cyclic response at the pile base in terms of lateral base force F_B and displacement y_B. Accumulated displacement Δy_B (normalised by $y_{B,0}$) increases linearly with the number of cycles in the bi-logarithmic space. Trends are consistent with those at the ground surface (Fig. 9c–d). The increase in $F_{B,N}$ with N (despite constant load amplitude) suggests progressive mobilisation of base resistance and highlights the need for cyclic hardening mechanisms in simplified base response models.

The base displacement behaviour is well captured by a power-law relation:

$$\frac{\Delta y_B}{y_{B,0}} = Y_{B,b} Y_{B,c} N^{Y_{B,\alpha}} \tag{4}$$

where $Y_{B,b}$, $Y_{B,c}$, and $Y_{B,\alpha}$ retain the same interpretation as in Eq. (2). For $\zeta_c = 0$, $Y_{B,c} = 1$. As with surface behaviour, $Y_{B,b}$ is expected to vary with ζ_b, relative density, and geometry—factors further explored in the final section of the paper. The FE data are well reproduced using $Y_{B,\alpha} = 0.55$, consistent with the values used to interpolate the response at ground surface.

Fig. 13 summarises the evolution of key reaction components during cyclic loading at $\zeta_b = 0.4$. The base force F_B and its moment contribution (M_{FB}) both increase with N, reflecting enhanced base engagement. While the resultant lateral soil force P also rises with

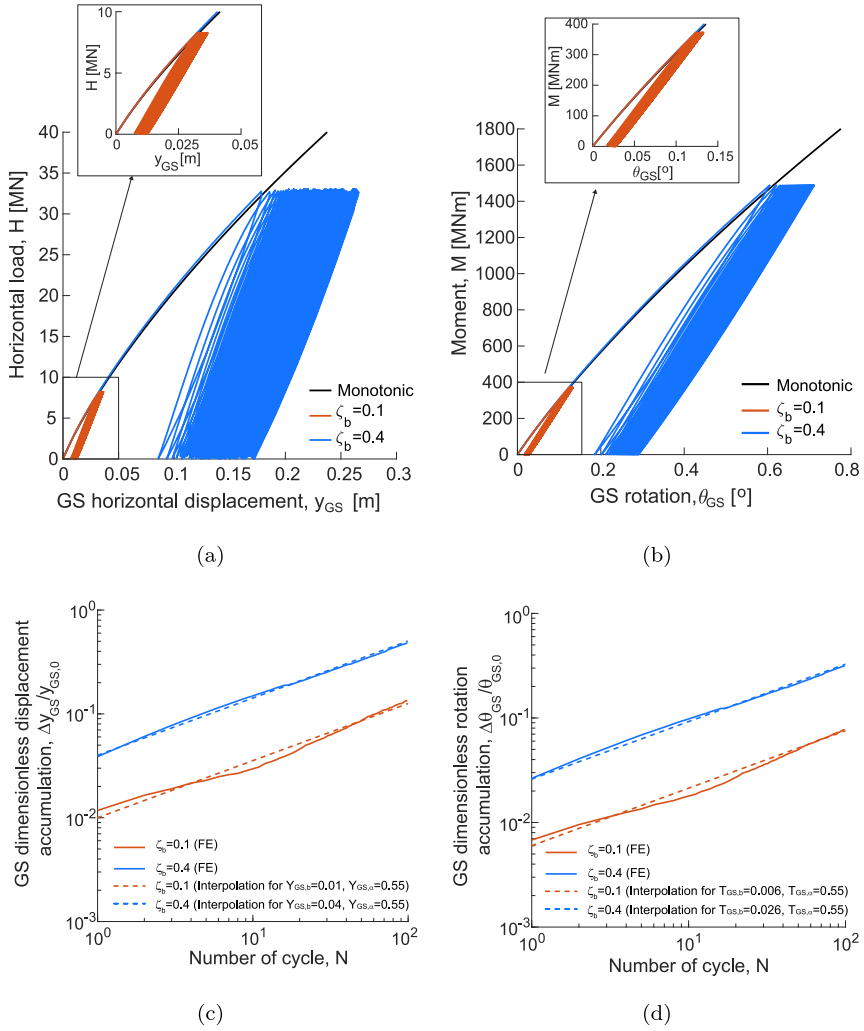


Fig. 9. Simulated monopile response at the ground surface under cyclic loading: (a) load–displacement and (b) moment–rotation curves; (c) accumulated lateral displacement; (d) accumulated rotation.

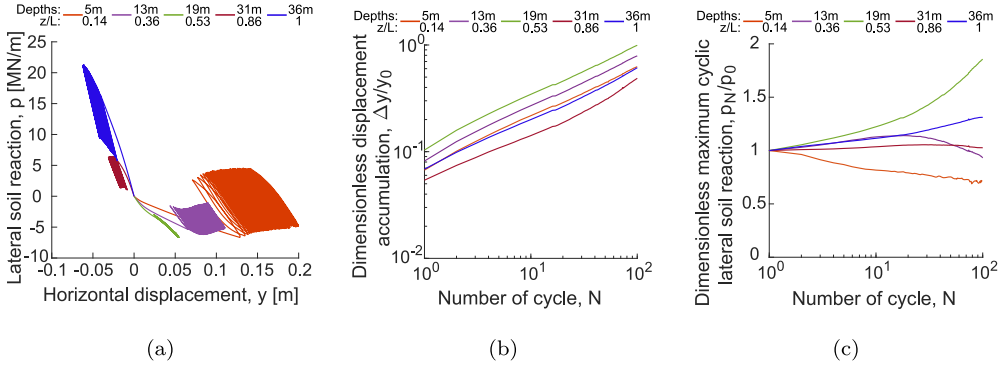


Fig. 10. Cyclic response at various depths for the case $\zeta_b = 0.4$: (a) p–y curves; (b) accumulated lateral displacements; (c) evolution of lateral soil reaction p_N normalised by initial value p_0.

cycles, its associated moment M_P decreases—indicative of stress redistribution towards the pile base. In contrast, the distributed moment M_D remains approximately constant despite local changes in m (see Fig. 11). This observation suggests that the cyclic dependence of m may be neglected in simplified models, without compromising the global moment balance. Finally, the base moment M_B continues to exhibit negligible influence even under sustained cycling.

4. Pile geometry–sand density interplay: parametric study

This section summarises the results of parametric 3D FE analyses aimed at investigating how monopile geometry and sand relative density affect pile behaviour (Table 3). Certain configurations – such as $D = 3$ m and $L/D = 1$ – are included as boundary cases rather and

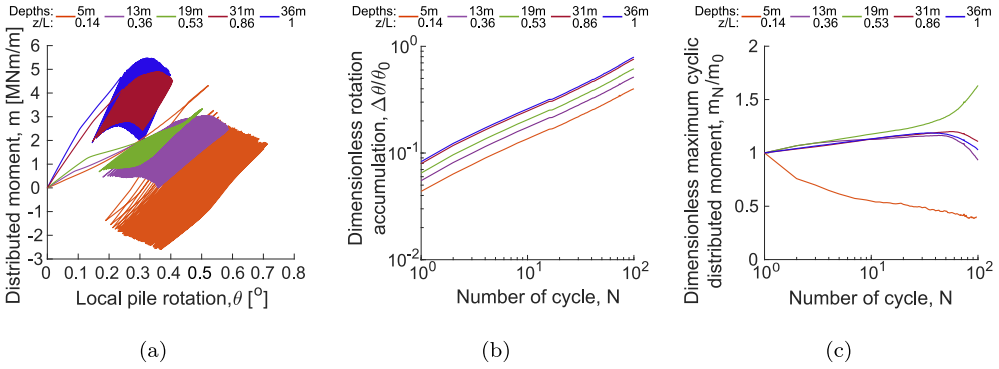


Fig. 11. Cyclic response for $\zeta_b = 0.4$: (a) m-θ curves at various depths, (b) cyclic accumulation of rotation, and (c) evolution of distributed moment m_N normalised by m_0.

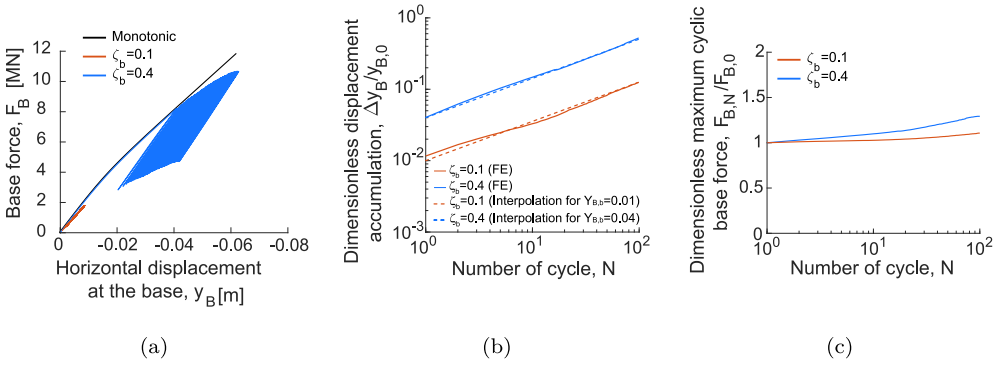


Fig. 12. Cyclic pile base response for $\zeta_b = 0.4$: (a) F_B-y_B curve, (b) accumulation of displacement $\Delta y_B/y_{B,0}$, and (c) evolution of base force $F_{B,N}/F_{B,0}$.

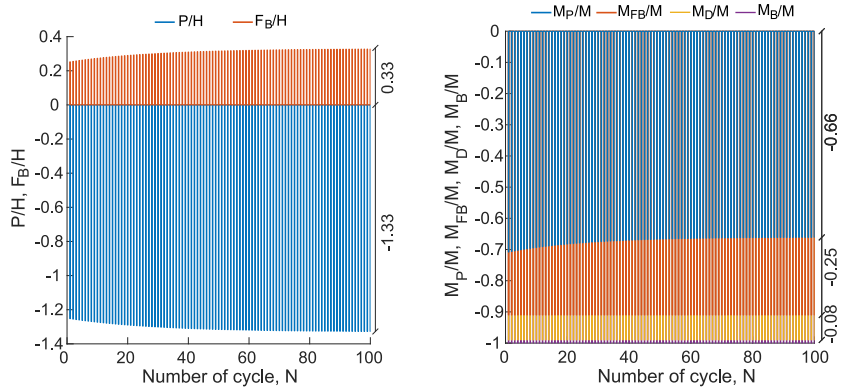


Fig. 13. Cyclic evolution of reaction resultants for $\zeta_b = 0.4$: (a) F_B and P normalised by H, (b) M_B, M_{FB}, M_P, and M_D normalised by $M = H \cdot h$.

are not representative of typical offshore wind turbine (OWT) monopile designs.

Both monotonic and cyclic responses broadly follow the trends previously discussed. The discussion here focuses on key summary metrics. For monotonic loading, attention is restricted to ultimate base force, base moment, and distributed moment, identifying when these components are significant. For cyclic loading, the accumulation of displacement and rotation is described using interpolation parameters from Eqs. (2), (3), and (4).

To establish a relationship between monopile response and its stiffness relative to the surrounding soil, the following non-dimensional flexibility factor, K_R^G, is adopted:

$$K_R^G = \frac{E_p I_p}{G L^4} \tag{5}$$

where $E_p I_p$ and G denote the pile flexural rigidity and the small-strain shear modulus of the soil at the pile base depth, respectively. This flexibility factor is essentially equivalent to the parameter K_R of Poulos (1982), defined using Young's modulus instead of G, through $K_R^G = 2(1+\nu)K_R$. Defining K_R^G in terms of G allows direct use of elastic stiffness measurements commonly obtained in offshore site investigations (e.g., geophysical surveys and seismic CPTs).

K_R^G indicates whether the pile exhibits rigid, flexible, or intermediate behaviour under lateral loading. Flexible piles typically mobilise

Table 3
Monopile geometries and sand relative densities considered in the 3D FE parametric study.

L/D \ D [m]	3	6	9	12
1	x	$D_r = 90\%$ $h/D = 5$	$D_r = 90\%$ $h/D = 5$	$D_r = 90\%$ $h/D = 5$
2	$D_r = 90\%$ $h/D = 5$	$D_r = 90\%$ $h/D = 5$	$D_r = 90\%$ $h/D = 5, 10$	$D_r = 90\%$ $h/D = 5$
4	$D_r = 90\%$ $h/D = 5$	$D_r = 90\%$ $h/D = 5, 10$	$D_r = 15, 30, 50, 90\%$ $h/D = 5, 10$	$D_r = 90\%$ $h/D = 5, 10$
6	$D_r = 90\%$ $h/D = 5$	$D_r = 90\%$ $h/D = 5$	$D_r = 90\%$ $h/D = 5$	$D_r = 90\%$ $h/D = 5$

negligible base reactions, whereas stiffer systems develop significant base resistance. This definition is directly related to the flexibility factor K_R introduced by Poulos (1982), which is formulated in terms of Young's modulus. The two measures are related through $K_R^G = 2(1+\nu)K_R$, enabling published threshold values to be readily converted once the Poisson's ratio ν is assumed or measured. Although the limiting values are not unique, several criteria have been proposed in the literature. For example, the rigid and flexible limits reported by Poulos (1982) are $K_R = 0.1$ and 10^{-5}, respectively. Other studies suggest comparable ranges (Poulos and Hull, 1989; He and Kaynia, 2024). While monopiles are often conceptualised as rigid and rotation-dominated (Achmus et al., 2009), practical designs typically fall within $K_R \sim 10^{-3}$–10^{-1} (or the equivalent K_R^G range), indicating intermediate behaviour in which both rotational and flexural mechanisms contribute.

Fig. 14 illustrates how normalised values of F_{Bu}, M_{Bu}, and M_{Du} vary with K_R^G. The following empirical fits offer good agreement (except for a few low-L/D outliers):

$$\frac{F_{Bu}}{H_u} = 1.35(K_R^G)^{0.35},\quad \frac{M_{Bu}}{M_u} = 0.075(K_R^G)^{0.35},\quad \frac{M_{Du}}{M_u} = 0.13(K_R^G)^{0.35} \tag{6}$$

These relationships allow rational assessment of when base and distributed moments should be included in simplified models. They also aid in interpreting small-scale test data and upscaling to real-world monopiles.

For cyclic cases, displacements and rotations were interpolated using Eqs. (2), (3), and (4), assuming $Y_{GS,c} = T_{GS,c} = Y_{B,c} = 1$. Bi-logarithmic plots showed nearly parallel trends, justifying a common exponent of 0.55 for $Y_{GS,\alpha}$, $T_{GS,\alpha}$, and $Y_{B,\alpha}$ across all cases. The coefficients $Y_{GS,b}$, $T_{GS,b}$, and $Y_{B,b}$ are functions of K_r^G.

Fig. 15 shows these coefficients normalised by ζ_b, consistent with findings by LeBlanc et al. (2010) and Liu et al. (2022), who observed linear scaling with ζ_b. Best-fit expressions are:

$$\frac{Y_{GS,b}}{\zeta_b} = 0.18(K_R^G)^{0.17},\quad \frac{T_{GS,b}}{\zeta_b} = 0.14(K_R^G)^{0.17},\quad \frac{Y_{B,b}}{\zeta_b} = 0.10 \tag{7}$$

which is generally consistent with the experimental observations of Wang et al. (2022b) regarding the effect of pile flexibility on global cyclic ratcheting behaviour. As in the monotonic case, deviations arise for low L/D configurations, which exhibit caisson-like behaviour. Nonetheless, the fitted relations remain promising tools for estimating cyclic accumulation using readily available parameters such as pile geometry, soil properties, and monotonic response data.

5. Conclusions

This paper presented a comprehensive numerical investigation of the monotonic and cyclic lateral response of piles embedded in dry sand. Soil behaviour was simulated using SANISAND-MS, an advanced constitutive model capable of capturing cyclic strain accumulation in granular materials. Model parameters were calibrated against centrifuge experiments. The analyses were intentionally restricted to relatively simple cyclic loading conditions, excluding asymmetric or irregular histories. Although these more complex scenarios were beyond the scope of the present work, they represent a natural extension for future research. The limited number of simulated cycles does not detract from the value of the adopted modelling framework, which enables detailed insight into the governing geotechnical mechanisms and provides a rational basis for mechanics-informed improvements to design approaches.

The main findings of the study can be summarised as follows:

- Under both monotonic and cyclic loading, the lateral soil reaction–displacement and distributed moment–local rotation relationships are not necessarily monotonic. This behaviour originates from localised soil–pile interaction mechanisms that are not readily captured by conventional one-dimensional soil reaction models.
- For the range of geometries considered, representative of monopiles currently used in practice, the base shear force, base moment, and distributed moment can contribute appreciably to the overall structural response, particularly to the rotational equilibrium of the monopile.
- The relative contribution of the base shear force increases slightly with the number of load cycles, whereas those of the distributed moment and base moment remain essentially unchanged, with the latter generally negligible for practical purposes.
- Irreversible displacements and rotations develop at both the ground surface and the pile base, evolving with the number of cycles according to a power-law relationship.

From a practical standpoint, the study introduced a simplified procedure to estimate the maximum contributions of base shear force, base moment, and distributed moment as a function of the relative pile–soil stiffness. This framework helps identify cases in which some contributions may be safely neglected, thereby reducing unnecessary modelling complexity.

In addition, a simple method was formulated to predict the cyclic accumulation of displacement and rotation at the ground surface and pile base under one-way cyclic loading. The method requires only the pile flexibility factor and the corresponding monotonic response, which can be obtained from analytical solutions or numerical analyses.

CRediT authorship contribution statement

Luca Flessati: Writing – review & editing, Writing – original draft, Supervision, Methodology, Formal analysis, Conceptualization. **Firman Habib:** Writing – original draft, Visualization, Software, Formal analysis. **Kuen-Wei Wu:** Supervision, Software, Methodology. **Haoyuan Liu:** Writing – review & editing, Validation, Supervision, Methodology, Investigation, Conceptualization. **Federico Pisanò:** Writing – review & editing, Writing – original draft, Software, Project administration, Methodology, Funding acquisition, Conceptualization.

Declaration of competing interest

The authors declare that they have no known competing financial interests or personal relationships that could have appeared to influence the work reported in this paper.

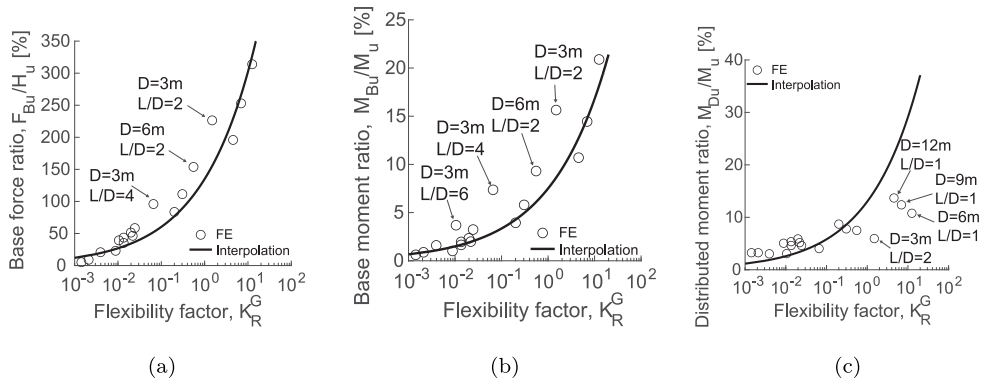


Fig. 14. Dependence of normalised base and distributed moments on K_R^G under monotonic loading: (a) F_{Bu}/H_u, (b) M_{Bu}/M_u, (c) M_{Du}/M_u.

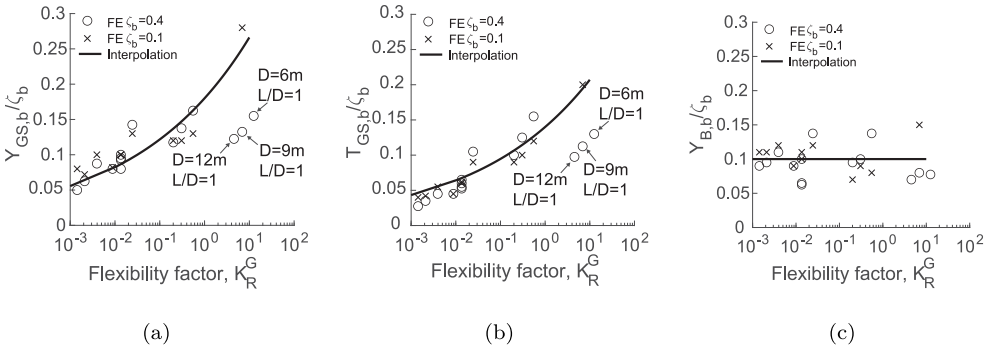


Fig. 15. Dependence of cyclic interpolation parameters on K_R^G: (a) $Y_{GS,b}/\zeta_b$, (b) $T_{GS,b}/\zeta_b$, (c) $Y_{B,b}/\zeta_b$.

Acknowledgements

MIDAS (Monopile Improved Design through Advanced cyclic Soil modelling) was an initiative developed as part of the GROW joint research programme. Funding from the Topsector Energiesubsidie of the Ministry of Economic Affairs and Climate Policy, Netherlands under RVO grant number TEHE111013 is gratefully acknowledged, along with support from the following partners (in alphabetical order): Delft University of Technology, Netherlands, Deltares, Netherlands, Eneco, Netherlands, Huisman, Netherlands, IHC, Netherlands, RWE, Netherlands, Shell, Netherlands, Siemens Gamesa, Netherlands, TotalEnergies, Netherlands, Van Oord, and Vattenfall, Netherlands. The MIDAS team expresses gratitude to NGI and DNV for their technical collaboration, with special acknowledgment of NGI's contribution through Federico Pisanò's continued involvement after his transition from TU Delft to NGI and Hans Petter Jostad's technical advice. The contribution of Ahmed Elkadi and Maria Konstadinou to project acquisition and management is greatly appreciated, as are the efforts of Rob Zwaan (Deltares) and Amin Askarinejad (TU Delft) in the centrifuge testing.

The corresponding author gratefully acknowledges the financial support provided by the Fundamental Research Funds for the Central Universities, China (Grant No. 501RCQD2025113003).

Appendix. Calibration and validation of the SANISAND-MS-based 3D FE model

This appendix summarises the calibration and validation of the adopted 3D finite element (FE) model incorporating the SANISAND-MS constitutive formulation. A comprehensive description is available in Liu et al. (2026), to which the reader is referred.

Table A.4
Initial confining pressure and void ratio for monotonic (CID) and cyclic (cycCAD) drained triaxial tests more details available in Liu et al. (2026).

Test type	Monotonic (CID)					Cyclic (CAD)	
Test ID	CID1	CID2	CID3	CID4	CID5	cycCAD1	cycCAD2
p_{in} [kPa]	55	205	406	205	207	50.8	400
e_{in} [–]	0.81	0.81	0.82	0.89	0.74	0.79	0.78

Experimental basis and calibration strategy

Model calibration and validation are based on an extensive experimental programme on Geba sand, comprising both element-scale tests and foundation-scale soil–structure interaction experiments. Table A.4 summarises the key test settings – namely the initial confining pressure, p_{in}, and void ratio, e_{in} – of the triaxial experiments that most directly supported the calibration of the SANISAND-MS parameters.

Parameter identification followed a two-stage procedure. Monotonic parameters were first derived from drained triaxial compression tests (CID) on isotropically consolidated specimens and validated against monotonic centrifuge results. Cyclic, memory-related parameters – most notably the ratcheting-control parameter μ_0 – were then obtained from drained cyclic triaxial tests (cycCAD) on anisotropically consolidated specimens and subsequently refined using cyclic centrifuge monopile data. This separation is enabled by the formulation of SANISAND-MS, in which the cyclic (memory) parameters do not affect the monotonic response.

The final parameter set reported in Table 1 can be shown to fall within the ranges established for comparable sands and previous applications of the SANISAND-MS model (Liu et al., 2019; Liu and Pisanò, 2019; Pisanò et al., 2024).

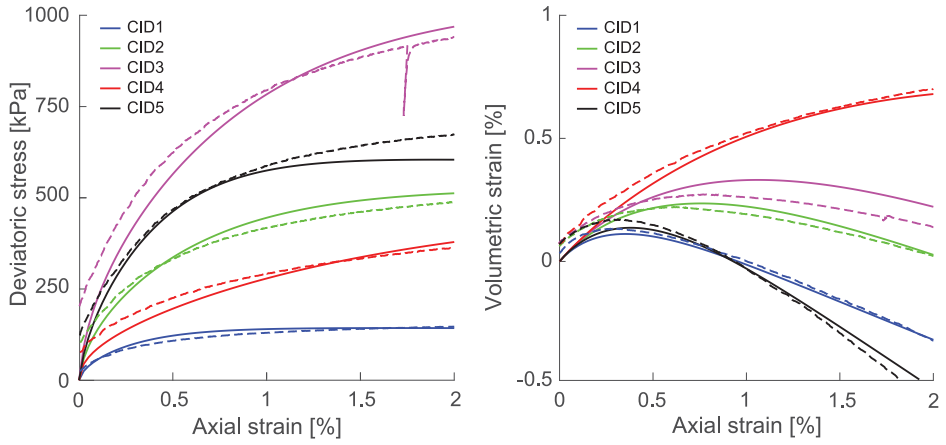


Fig. A.1. SANISAND-MS model calibrated against drained triaxial tests, focusing on axial strains up to 2%. Dashed lines: experiments; solid lines: SANISAND-MS simulations.

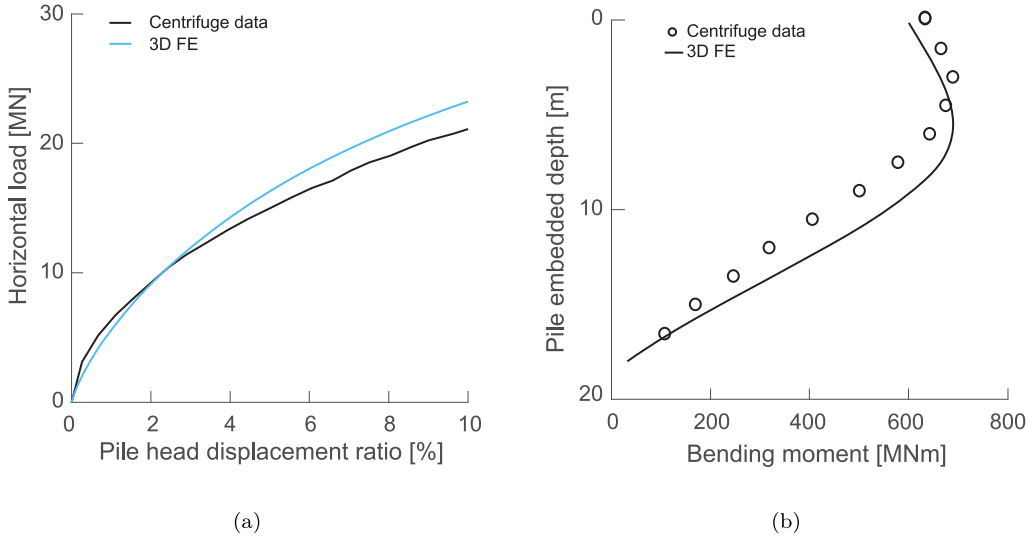


Fig. A.2. Comparison of monotonic centrifuge test measurements and 3D FE numerical simulations: (a) load–displacement response; (b) bending-moment distribution with depth.

Monotonic behaviour and calibration of governing parameters

The monotonic CID1-5 triaxial tests listed in Table A.4 are shown in Fig. A.1 (dashed lines) in terms of deviatoric stress vs. axial strain and volumetric strain vs. axial strain responses.

The parameter set reported in Table 1 (from G_0 to n^d) was identified with emphasis on intermediate strain levels (typically below 2%–5%), consistent with centrifuge evidence and previous numerical back-analyses indicating that this range governs monopile lateral behaviour under operational and serviceability conditions. Element-level simulations performed with SANISAND-MS (solid lines in Fig. A.1) reproduce both the stress–strain response and volumetric trends with good accuracy within this regime. Larger strains remain reasonably captured but were not a primary calibration target (Liu et al., 2026).

The quality of the resulting parameter set was further assessed against foundation-scale behaviour using centrifuge data from Peccin da Silva et al. (2026). For brevity, only one representative test is discussed here (100 g; modelled prototype dimensions: $D = 6\,\text{m}$, $L = 18\,\text{m}$, $h = 25\,\text{m}$, $t_p = 0.2\,\text{m}$, $D_r = 96.7\%$), while the complete validation exercise is documented in Liu et al. (2026).

Fig. A.2a compares the measured and FE-simulated load–displacement curves, with displacement normalised by the pile diameter. The model reproduces both the initial stiffness and the overall response shape within the serviceability range, with only a slight overestimation of the ultimate capacity at larger displacements. Complementary insight is provided by the bending-moment profiles in Fig. A.2b, where the numerical results capture the depth, magnitude, and distribution of the peak moments with satisfactory agreement.

Cyclic behaviour and calibration of memory parameters

The calibration of the memory parameters governing cyclic behaviour (particularly μ_0) was first performed using the cycCAD1-2 triaxial tests listed in Table A.4, and subsequently refined against cyclic centrifuge data. The responses from the two cyclic triaxial tests are

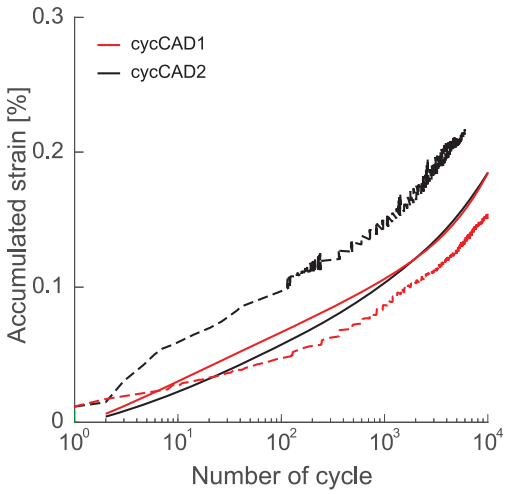


Fig. A.3. Comparison of cyclic triaxial test results (dashed lines) and SANISAND-MS predictions with $\mu_0 = 100$ (solid lines).

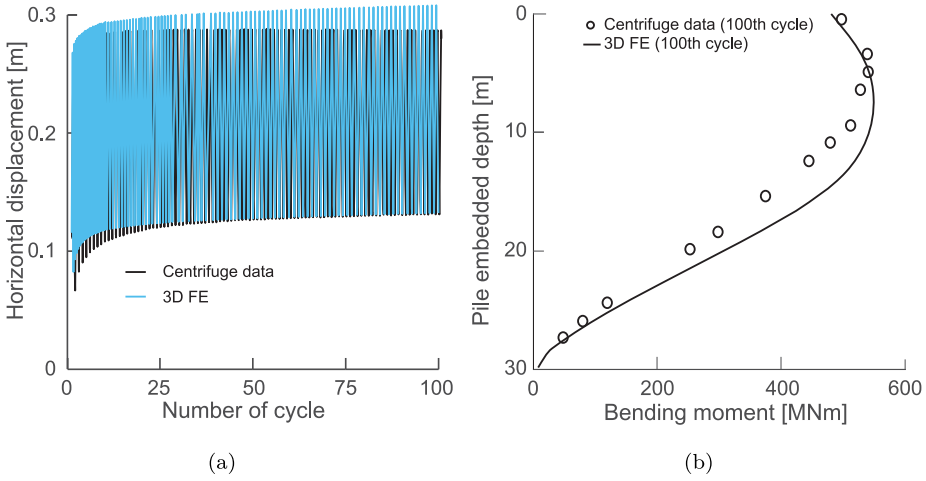


Fig. A.4. Comparison of cyclic centrifuge test measurements and numerical predictions (with $\mu_0 = 500$): (a) accumulated ground-surface displacement; (b) bending-moment distribution with depth after 100 cycles.

shown in Fig. A.3 (dashed lines) in terms of accumulated total strain[3] versus number of cycles. In test cycCAD2, the final accumulated strain exceeds that of cycCAD1, indicating a stress-dependent accumulation trend. SANISAND-MS simulations (solid lines, parameters from Table 1 with $\mu_0 = 100$) display only limited pressure sensitivity. Experimental evidence remains mixed, with Wichtmann (2016) reporting nearly pressure-independent accumulation and Wichtmann et al. (2017) observing clear stress dependence. Overall, the numerical response shows reasonable agreement with the element tests.

Given the inherent complexity of cyclic triaxial testing and the possibility that fabric changes induced by deposition and pile installation differ from those captured at the element scale (Staubach et al., 2020; Fan et al., 2021), the cyclic parameters were further constrained using centrifuge monopile experiments. Results from a 100 g test in 99% dense sand (modelled prototype dimensions: $D = 6,\mathrm{m}$, $L = 30,\mathrm{m}$, $h = 30,\mathrm{m}$, $t_p = 0.2,\mathrm{m}$) were compared with corresponding simulations using $\mu_0 = 100$. Although the overall response was qualitatively well-captured, the accumulation of pile-head displacement was overpredicted. Increasing μ_0 to 500 (Table 1) mitigated this effect and improved the agreement in terms of accumulated displacements (Fig. A.4a). The corresponding bending-moment profiles after 100 cycles (Fig. A.4b) are also captured with satisfactory accuracy. The final parameter set in Table 1 was therefore deemed adequate to support the parametric studies presented in this paper.

[3] $\varepsilon^{\mathrm{acc}} = \sqrt{(\varepsilon_a^{\mathrm{acc}})^2 + 2(\varepsilon_r^{\mathrm{acc}})^2}$, where $\varepsilon_a^{\mathrm{acc}}$ and $\varepsilon_r^{\mathrm{acc}}$ denote the accumulated axial and radial accumulated strains, respectively.

Data availability

Data can be made available upon reasonable request.

References

Abadie, C.N., Beuckelaers, W.J., Byrne, B.W., Houlsby, G.T., Burd, H.J., McAdam, R., 2023. Modeling lifetime performance of monopile foundations for offshore wind applications. J. Geotech. Geoenvironmental Eng. 149 (8), 04023051.

Abadie, C.N., Byrne, B.W., Houlsby, G.T., 2019. Rigid pile response to cyclic lateral loading: laboratory tests. Géotechnique 69 (10), 863–876.

Abu-Kassab, Q., Suleiman, M.T., Ricles, J.M., Sause, R., Marullo, T., 2025. Large-scale multidirectional soil-foundation-structure interaction testing of renewable energy systems. Ocean Eng. 323, 120595.

Achmus, M., Kuo, Y.-S., Abdel-Rahman, K., 2009. Behavior of monopile foundations under cyclic lateral load. Comput. Geotech. 36 (5), 725–735.

Achmus, M., Schmoor, K.A., Herwig, V., Matlock, B., 2020. Lateral bearing behaviour of vibro- and impact-driven large-diameter piles in dense sand. Geotechnik 43 (3), 147–159.

API, 2010. Recommended practice 2A-WSD planning, designing, and constructing fixed offshore platforms.

Been, K., Jefferies, M.G., 1985. A state parameter for sands. Géotechnique 35 (2), 99–112.
Beuckelaers, W., Burd, H., Houlsby, G., McAdam, R., Byrne, B., 2020. A generalised Winkler model for the hysteretic and ratcheting behaviour of monopiles in clay and sand. In: Frontiers in Offshore Geotechnics IV: Proceedings of the 4th International Symposium on Frontiers in Offshore Geotechnics. ISFOG 2021.
Burd, H.J., Taborda, D.M., Zdravković, L., Abadie, C.N., Byrne, B.W., Houlsby, G.T., Gavin, K.G., Igoe, D.J., Jardine, R.J., Martin, C.M., et al., 2020. PISA design model for monopiles for offshore wind turbines: application to a marine sand. Géotechnique 70 (11), 1048–1066.
Byrne, B.W., Aghakouchak, A., Buckley, R.M., Burd, H.J., Gengenbach, J., Houlsby, G.T., McAdam, R.A., Martin, C.M., Schranz, F., Sheil, B.B., et al., 2020a. PICASO: cyclic lateral loading of offshore wind turbine monopiles. In: Frontiers in Offshore Geotechnics IV: Proceedings of the 4th International Symposium on Frontiers in Offshore Geotechnics (ISFOG 2020).
Byrne, B.W., Burd, H.J., Zdravkovic, L., Abadie, C.N., Houlsby, G.T., Jardine, R.J., Martin, C.M., McAdam, R.A., Pacheco Andrade, M., Pedro, A.M., et al., 2019. PISA design methods for offshore wind turbine monopiles. In: Offshore Technology Conference. OTC, D011S005R002.
Byrne, B.W., McAdam, R.A., Beuckelaers, W.J.A.P., Burd, H.J., Gavin, K., Houlsby, G.T., Igoe, D.J.P., Jardine, R., Martin, C.M., et al., 2020b. Cyclic laterally loaded medium-scale field pile testing for the PISA project. In: Frontiers in Offshore Geotechnics IV: Proceedings of the 4th International Symposium on Frontiers in Offshore Geotechnics (ISFOG 2020). pp. 1323–1332.
Cheng, X., Ibraim, E., Liu, H., Pisanò, F., Diambra, A., 2023. Large diameter laterally loaded piles in sand: Numerical evaluation of soil stress paths and relevance of laboratory soil element testing. Comput. Geotech. 154, 105139.
Corciulo, S., Zanoli, O., Pisanò, F., 2017. Transient response of offshore wind turbines on monopiles in sand: role of cyclic hydro–mechanical soil behaviour. Comput. Geotech. 83, 221–238.
Corti, R., Diambra, A., Wood, D.M., Escribano, D.E., Nash, D.F., 2016. Memory surface hardening model for granular soils under repeated loading conditions. J. Eng. Mech. 142 (12), 04016102.
Dafalias, Y.F., Manzari, M.T., 2004. Simple plasticity sand model accounting for fabric change effects. J. Eng. Mech. 130 (6), 622–634.
DNV, 2016. DNV-GL-ST-0126 support structures for wind turbines.
Fan, S., Bienen, B., Randolph, M.F., 2021. Effects of monopile installation on subsequent lateral response in sand. II: Lateral loading. J. Geotech. Geoenvironmental Eng. 147 (5), 04021022.
Fuentes, W., Gil, M., Rivillas, G., 2021. A p–y model for large diameter monopiles in sands subjected to lateral loading under static and long-term cyclic conditions. J. Geotech. Geoenvironmental Eng. 147 (2), 04020164.
He, R., Kaynia, A.M., 2024. Winkler spring coefficients for laterally loaded piles. Comput. Geotech. 170, 106264.
Higgins, W., Vasquez, C., Basu, D., Griffiths, D., 2013. Elastic solutions for laterally loaded piles. J. Geotech. Geoenvironmental Eng. 139 (7), 1096–1103.
Houlsby, G.T., 2016. Interactions in offshore foundation design. Géotechnique 66 (10), 791–825.
Houlsby, G.T., Abadie, C.N., Beuckelaers, W.J., Byrne, B.W., 2017. A model for nonlinear hysteretic and ratcheting behaviour. Int. J. Solids Struct. 120, 67–80.
Hu, Q., Han, F., Prezzi, M., Salgado, R., Zhao, M., 2022. Lateral load response of large-diameter monopiles in sand. Géotechnique 72 (12), 1035–1050.
Jostad, H.P., Liu, H., Sivasithamparam, N., Ragni, R., 2023. Cyclic capacity of monopiles in sand under partially drained conditions: a numerical approach. J. Geotech. Geoenvironmental Eng. 149 (2), 04022129.
Kementzetzidis, E., Pisanò, F., Elkadi, A.S., Tsouvalas, A., Metrikine, A.V., 2023a. Gentle Driving of Piles (GDP) at a sandy site combining axial and torsional vibrations: Part II-cyclic/dynamic lateral loading tests. Ocean Eng. 270, 113452.
Kementzetzidis, E., Pisanò, F., Metrikine, A.V., 2022. A memory-enhanced py model for piles in sand accounting for cyclic ratcheting and gapping effects. Comput. Geotech. 148, 104810.
Kementzetzidis, E., Pisanò, F., Tsetas, A., Metrikine, A.V., 2023b. Gentle Driving of Piles at a sandy site combining axial and torsional vibrations: quantifying the influence of pile installation method on lateral behavior. J. Geotech. Geoenvironmental Eng. 149 (11), 04023102.
Klinkvort, R.T., Hededal, O., 2013. Lateral response of monopile supporting an offshore wind turbine. Proc. Inst. Civ. Engineers-Geotechnical Eng. 166 (2), 147–158.
LeBlanc, C., Houlsby, G.T., Byrne, B.W., 2010. Response of stiff piles in sand to long-term cyclic lateral loading. Géotechnique 60 (2), 79–90.
Li, Q., Askarinejad, A., Gavin, K., 2022. Lateral response of rigid monopiles subjected to cyclic loading: centrifuge modelling. Proc. Inst. Civ. Engineers-Geotechnical Eng. 175 (4), 426–438.
Li, Z., Del Brocco, I., Hicks, M.A., Pisanò, F., 2026. Enhanced SANISAND-MS model implementation for robust 3D FE analysis of cyclically loaded foundations. (submitted for publication).
Li, W., Igoe, D., Gavin, K., 2014. Evaluation of CPT-based p-y models for laterally loaded piles in siliceous sand. Géotechnique Lett. 4 (2), 110–117.
Li, W., Igoe, D., Gavin, K., 2015. Field tests to investigate the cyclic response of monopiles in sand. Proc. Inst. Civ. Engineers-Geotechnical Eng. 168 (5), 407–421.
Li, Z., Kotronis, P., Escoffier, S., Tamagnini, C., 2016. A hypoplastic macroelement for single vertical piles in sand subject to three-dimensional loading conditions. Acta Geotech. 11, 373–390.
Li, Z., Liu, H., Hicks, M.A., Pisanò, F., 2023. Influence of static–cyclic load misalignment on the drained tilting response of offshore monopiles in sand. Comput. Geotech. 156, 105306.
Li, Q., Ming, J., Wen, K., Wang, K., Ma, Q., Cheng, X., Zhang, Y., 2025. Long-term scouring effects on the lateral loading behaviour of monopiles using field monitoring data and finite element modelling. Appl. Ocean Res. 165, 104821.
Little, R., Briaud, J., 1988. Full scale cyclic lateral load tests on six single piles in sand. Miscellaneous Paper GL-88-27, Geoteehnical Div., Texas AMUniv., College Station, Tex.
Liu, H.Y., Abell, J.A., Diambra, A., Pisanò, F., 2019. Modelling the cyclic ratcheting of sands through memory-enhanced bounding surface plasticity. Geotechnique 69 (9), 783–800.
Liu, H.Y., Gong, F., Zhao, H., 2026a. Influence of load idealisation on strain and pore pressure accumulation in clay. Géotechnique Lett. 1–8.
Liu, H.Y., Kementzetzidis, E., Abell, J.A., Pisanò, F., 2022. From cyclic sand ratcheting to tilt accumulation of offshore monopiles: 3D FE modelling using SANISAND-MS. Géotechnique 72 (9), 753–768.
Liu, H.Y., Konstadinou, M., Wang, H., Jostad, H.P., Pisanò, F., 2026. 3D FE cyclic modelling of monopiles in sand using SANISAND-MS: calibration and validation from soil element to pile-interaction scale. Soil Dyn. Earthq. Eng. 204, 110177.
Liu, H.Y., Nagula, S., Jostad, H.P., Piciullo, L., Nadim, F., 2024. Considerations for using critical state soil mechanics based constitutive models for capturing static liquefaction failure of tailings dams. Comput. Geotech. 167, 106089.
Liu, H.Y., Pisanò, F., 2019. Prediction of oedometer terminal densities through a memory-enhanced cyclic model for sand. Géotechnique Lett. 9 (2), 81–88.
Long, J., Vanneste, G., 1994. Effects of cyclic lateral loads on piles in sand. J. Geotech. Eng. 120 (1), 225–244.
McAdam, R.A., Byrne, B.W., Houlsby, G.T., Beuckelaers, W.J., Burd, H.J., Gavin, K.G., Igoe, D.J., Jardine, R.J., Martin, C.M., Muir Wood, A., et al., 2020. Monotonic laterally loaded pile testing in a dense marine sand at Dunkirk. Géotechnique 70 (11), 986–998.
Page, A.M., Grimstad, G., Eiksund, G.R., Jostad, H.P., 2018. A macro-element pile foundation model for integrated analyses of monopile-based offshore wind turbines. Ocean Eng. 167, 23–35.
Page, A.M., Grimstad, G., Eiksund, G.R., Jostad, H.P., 2019. A macro-element model for multidirectional cyclic lateral loading of monopiles in clay. Comput. Geotech. 106, 314–326.
Peccin da Silva, A., Wang, H., Zwaan, R., Askarinejad, A., Pisanò, F., 2026. Cyclic lateral behaviour of monopiles in very dense sand: a centrifuge study on pile geometry and loading sequence effects. (submitted for publication).
Pisanò, F., 2019. Input of advanced geotechnical modelling to the design of offshore wind turbine foundations. In: The XVII European Conference on Soil Mechanics and Geotechnical Engineering. Icelandic Geotechnical Society (IGS), pp. 272–297.
Pisanò, F., Askarinejad, A., Wang, H., Maghsoodi, S., Gavin, K., Segeren, M., Elkadi, A., de Lange, D., Konstadinou, M., 2022. MIDAS: Monopile improved design through advanced cyclic soil modelling. In: Proceedings of 20th International Conference on Soil Mechanics and Geotechnical Engineering. ICSMGE2022, Sydney, Australia.
Pisanò, F., Del Brocco, I., Ho, H., Brasile, S., 2024. 3D FE simulation of PISA monopile field tests at Dunkirk using SANISAND-MS. Géotechnique Lett. 1–30.
Pisanò, F., Kementzetzidis, E., Wang, H., Marino, M., Zwaan, R., Peccin da Silva, A., Konstadinou, M., Elkadi, A., Liu, H., Askarinejad, A., Jostad, H.P., 2025. Testing and modelling of cyclic monopile behaviour in sand: highlights and insights from the MIDAS project. In: Proceedings of ISFOG 2025: 5th International Symposium on Frontiers in Offshore Geotechnics. Nantes, France.
Poulos, H.G., 1982. Single pile response to cyclic lateral load. J. Geotech. Eng. Div. 108 (3), 355–375.
Poulos, H.G., Hull, T.S., 1989. The role of analytical geomechanics in foundation engineering. In: Foundation Engineering: Current Principles and Practices. ASCE, pp. 1578–1606.
Reese, L., Cox, W., Koop, F., 1974. Analysis of laterally loaded piles in sand. In: Offshore Technology in Civil Engineering Hall of Fame Papers from the Early Years, OTC. Vol. 2080.
Richards, I.A., Byrne, B.W., Houlsby, G.T., 2020. Monopile rotation under complex cyclic lateral loading in sand. Géotechnique 70 (10), 916–930.
Roy, A., Liu, H., Bienen, B., Chow, S., Diambra, A., 2024. Suction bucket performance in sand under vertical cyclic loading: Numerical modelling using SANISAND-MS. Comput. Geotech. 173, 106497.
Stastny, A., Medicus, G., Galavi, V., Tafili, M., Tschuchnigg, F., 2025. Evaluation of advanced soil models for the cyclic soil-structure interaction of integral bridges. Acta Geotech. 1–26.
Staubach, P., Machaček, J., Moscoso, M., Wichtmann, T., 2020. Impact of the installation on the long-term cyclic behaviour of piles in sand: A numerical study. Soil Dyn. Earthq. Eng. 138, 106223.
Staubach, P., Wichtmann, T., 2020. Long-term deformations of monopile foundations for offshore wind turbines studied with a high-cycle accumulation model. Comput. Geotech. 124, 103553.

Taborda, D.M., Zdravković, L., Potts, D.M., Burd, H.J., Byrne, B.W., Gavin, K.G., Houlsby, G.T., Jardine, R.J., Liu, T., Martin, C.M., et al., 2020. Finite-element modelling of laterally loaded piles in a dense marine sand at Dunkirk. Géotechnique 70 (11), 1014–1029.

Wang, H., Lehane, B., Bransby, M., Wang, L., Hong, Y., 2022a. Field and numerical study of the lateral response of rigid piles in sand. Acta Geotech. 17 (12), 5573–5584.

Wang, Y., Zhu, M.-X., Gong, W.-M., Dai, G.-L., Wu, J.-B., Zhu, W.-B., 2022b. Cyclic lateral responses of monopiles considering the influence of pile—soil relative stiffness in sand. China Ocean Eng. 36 (2), 247–257.

Wang, H., Zwaan, R., Peccin da Silva, A., Askarinejad, A., Pisanò, F., 2025. Physical modelling of cyclically loaded monopiles in sand: the MIDAS centrifuge testing programme. In: 5th International Symposium on Frontiers in Offshore Geotechnics, ISFOG 2025. International Society for Soil Mechanics and Geotechnical Engineering.

Wen, K., White, D.J., Cerfontaine, B., Gourvenec, S., Diambra, A., 2025. Interpretative framework for CPT py module tests in drained sands: a practical model for end effect elimination considering sand relative density and surcharge pressure. Comput. Geotech. 183, 107205.

Wichtmann, T., 2016. Soil behaviour under cyclic loading: experimental observations, constitutive description and applications. Karlsruhe Institute of Technology (KIT), Karlsruhe, Germany, Habilitation thesis.

Wichtmann, T., Triantafyllidis, T., Chrisopoulos, S., Zachert, H., 2017. Prediction of long-term deformations of offshore wind power plant foundations using HCA-based engineer-oriented models. Int. J. Offshore Polar Eng. 27 (04), 346–356.

Zha, X., Guo, Z., Wang, L., Rui, S., 2022. A simplified model for predicting the accumulated displacement of monopile under horizontal cyclic loadings. Appl. Ocean Res. 129, 103389.

Zhang, W., Askarinejad, A., 2019. Centrifuge modelling of submarine landslides due to static liquefaction. Landslides 16 (10), 1921–1938.